2023

Classification and Characterization of Damage in Composite Laminates Using Electrical Resistance Tomography and Supervised Machine Learning

Julia Diaz-Escobar
Tecnológico Nacional de México

Paulina Díaz-Montiel
University of San Diego

Satchi Venkataraman
San Diego State University

Arnoldo Díaz-Ramirez
Tecnológico Nacional de México

Classification and Characterization of Damage in Composite Laminates Using Electrical Resistance Tomography and Supervised Machine Learning

Abstract

Electrical resistance tomography (ERT) is a nondestructive evaluation technique that uses the internal conductivity variations of materials to assess structural integrity. Due to the low instrumentation required, the widespread use of ERT in the aerospace industry for monitoring the accumulation of damage in aircraft components can lead to significant reductions in inspections and maintenance costs. However, implementing the ERT method for mapping the damage state of structural components made of carbon fiber reinforced polymeric (CFRP) composites is challenging due to the inability of this method to distinguish between damage modes such as delamination and matrix cracking. This article explores the combined use of ERT and machine learning algorithms such as neural networks, random forests, k-nearest neighbors, and support vector machines to classify and characterize delamination and matrix cracking damage in CFRP laminates. Results show that the proposed classification algorithms can successfully estimate the damage severity of delaminated composites in the presence of matrix cracking. Similarly, the classification algorithms can characterize these independent damage modes with an accuracy of 95%. The algorithms showed robustness to predict the electrical resistance variations of damaged composites and characterize delamination and matrix cracking damage even when intrinsic noise was considered. Although neural networks characterized damage with the highest accuracy, these algorithms were also the most sensitive to noise. For applications where instrumentation noise cannot be completely removed from the ERT signals, the use of nearest neighbors is thus recommended.

Hindawi
Structural Control and Health Monitoring
Volume 2023, Article ID 1675867, 19 pages
https://doi.org/10.1155/2023/1675867

Research Article

Classification and Characterization of Damage in Composite Laminates Using Electrical Resistance Tomography and Supervised Machine Learning

Julia Diaz-Escobar,[1] **Paulina Díaz-Montiel**,[2] **Satchi Venkataraman**,[3] **and Arnoldo Díaz-Ramírez**[1]

[1]*Department of Computer Systems, Tecnológico Nacional de México, IT de Mexicali, Mexicali, BC 21376, Mexico*
[2]*Department of Mechanical Engineering, University of San Diego, 5998 Alcala Park, San Diego, CA 92110-2492, USA*
[3]*Department of Aerospace Engineering, San Diego State University, 5500 Campanile Dr., San Diego, CA 92182, USA*

Correspondence should be addressed to Arnoldo Díaz-Ramírez; adiaz@itmexicali.edu.mx

Received 19 September 2022; Accepted 19 October 2022; Published 8 February 2023

Academic Editor: Young-Jin Cha

Electrical resistance tomography (ERT) is a nondestructive evaluation technique that uses the internal conductivity variations of materials to assess structural integrity. Due to the low instrumentation required, the widespread use of ERT in the aerospace industry for monitoring the accumulation of damage in aircraft components can lead to significant reductions in inspections and maintenance costs. However, implementing the ERT method for mapping the damage state of structural components made of carbon fiber reinforced polymeric (CFRP) composites is challenging due to the inability of this method to distinguish between damage modes such as delamination and matrix cracking. This article explores the combined use of ERT and machine learning algorithms such as neural networks, random forests, k-nearest neighbors, and support vector machines to classify and characterize delamination and matrix cracking damage in CFRP laminates. Results show that the proposed classification algorithms can successfully estimate the damage severity of delaminated composites in the presence of matrix cracking. Similarly, the classification algorithms can characterize these independent damage modes with an accuracy of 95%. The algorithms showed robustness to predict the electrical resistance variations of damaged composites and characterize delamination and matrix cracking damage even when intrinsic noise was considered. Although neural networks characterized damage with the highest accuracy, these algorithms were also the most sensitive to noise. For applications where instrumentation noise cannot be completely removed from the ERT signals, the use of nearest neighbors is thus recommended.

1. Introduction

Carbon fiber reinforced polymeric (CFRP) composites are high-performance materials widely used in the aerospace industry due to their excellent mechanical properties such as durability, fatigue resistance, and high stiffness-to-strength ratios. Despite the advanced structural performance, very few industry standards currently outline the critical damage threats for composites. This lack of industry standards is partly due to the lack of design criteria and comprehensive analysis protocols for the complete damage-tolerance evaluation of these materials. Consequently, certification and design of primary and secondary composite aircraft structural components must comply with the damage-tolerance requirement, which entails demonstrating a reliable service life while retaining at least limited load capability in the presence of damage (category of damage 1 and 2). Damage should not grow or, if slow or arrested growth occurs, the level of residual strength retained must be sufficiently above the limit load capability [1].

To assess damage threats in aircraft composite structural components and comply with the damage-tolerance

requirement, rigorous inspections and maintenance programs must be adopted to ensure structural integrity. However, it is estimated that the inspection and maintenance costs can account for more than 27% of the total life cycle cost of the aircraft [2]. In 2019, the global maintenance, repair, and overhaul (MRO) market accounted for 10.3% of airlines' operational costs [3]. One solution to reduce maintenance expenditures is to adopt a condition-based maintenance (CBM) approach, where the aircraft's health status is monitored at certain time intervals. If the safety of the system at any point is jeopardized, maintenance is then requested and conducted [4]. In CBM, the health status of the structure can be monitored using different structural health monitoring (SHM) techniques.

The electrical resistance tomography (ERT) is a SHM and nondestructive evaluation (NDE) technique that uses the electrical conductivity variations in materials to assess the structural integrity. It is an advantageous method because of the low instrumentation and costs required for implementation, and it can be particularly beneficial for monitoring the damage state of aircraft components during the scheduled inspections between flights. ERT is an imaging technique that reconstructs the in-plane conductivity inside the material after undergoing electrical excitation (forward problem). Damage identification is possible by solving the inverse problem, which requires reconstruction of the internal conductivity from boundary voltage measurements taken at the surface electrodes. Given the undamaged conductivity field, the damage parameters can be identified by evaluating the conductivity variations. A schematic of the ERT problem for identification of damage in structural components is shown in Figure 1. The figure also shows the two-probe method, which uses the same pair of surface electrodes for injecting electrical current and measuring the boundary potential.

Since CFRP composites are highly conductive in the fiber direction, the ERT method can be used to evaluate the structural integrity using the electrical conductivity variations these materials exhibit in the presence of damage. The capabilities of the ERT method for SHM of composites have been demonstrated for traditional CFRP laminates [5–9] as well as for composites with nano-reinforcements and conductive coatings [10–13]. The most recent advances in ERT for SHM of composites are thoroughly described in the topical review by Tallman and Smyl [14].

For composites, the ERT inverse problem is typically ill-conditioned since different conductivity distributions can lead to the same boundary voltage data. Additionally, reconstruction of the in-plane conductivity fields is computationally demanding because of the anisotropic conductivity properties of these materials. Although highly conductive in the fiber direction, the electrical conductivity of composites in the directions transverse and normal to the fibers is two to three orders of magnitude lower, making the inverse identification of damage more challenging. Another problem is the through-the-thickness localization of damage in composite laminates. The traditional formulation of the ERT inverse problem uses in-plane conductivity distribution fields to map the internal damage. However, these electrical

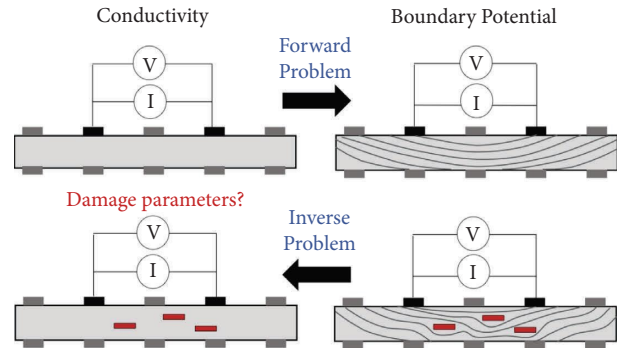

Figure 1: Schematic of the ERT and two-probe methodology for identification and characterization of damage.

variations are insufficient to characterize the damage's interlaminar location (i.e., delamination), and thus requires extensive experimental data for accurate detection.

The integration of artificial intelligence and NDE techniques proposes a new paradigm for diagnosing the damage state of composite structures and the prognosis of the remaining service life. Within the ERT framework, machine learning (ML) tools can be employed to describe the electrical behavior of composites and to characterize damage signatures in the laminates based on boundary voltage measurements. The ERT method and different ML techniques have been successfully used in chemical applications [15], two-phase materials [16, 17], concrete structures [18, 19], and industrial processes [20]. ML models developed to assess the structural integrity of composite structures have also been proposed based on vibrational signals [21, 22], wave propagation [23], and signals from piezoelectric sensors [24]. The review by Elenchezhian et al. summarizes the state-of-the-art for integrating ML and NDE methods for diagnosis of damage in composites [25].

In only a few studies, ML algorithms have been used along with the ERT method to describe the internal damage state of composites. Schmidt [26] proposed classification algorithms to infer the presence of delamination cracks and cavities in composite laminates. The algorithms studied included neural networks (NN), k-nearest neighbors (KNN), random forest (RF), and support vector machines (SVM). The problem was treated as a binary classification problem, and the results showed these algorithms could successfully predict the presence of such defects. In addition to the detection and classification of damage, it is desired that the proposed ML tools can also accurately characterize the state of internal damage. To this end, regression algorithms are required. Neural networks have been employed in the past to characterize delamination cracks in composite structures using ERT [27, 28]. Other surrogate modeling techniques employed for damage identification in composites include response surfaces [6, 29, 30], nonuniform rational *B*-splines [31], and Kriging surrogates [32, 33].

The models described above were capable of characterizing delamination location and size. However, accurate representation of the internal damage state of a composite laminate also requires quantification of the matrix cracking

damage mode, as these cracks reduce the transverse and shear strength of composites, leading to interlaminar failure [34]. Diaz-Montiel et al. [35] used a surrogate-based optimization approach for assessing the damage state of composites with both delamination and transverse matrix cracking using Kriging surrogates. These metamodeling techniques successfully characterized delamination cracks in the presence of matrix cracking, but they could not accurately describe the homogenized effect of the matrix cracking density on the electrical variations measured at the surface electrodes.

This research explores the use of ML algorithms to identify, classify, and characterize damage in composites using ERT. The ML algorithms must provide a low detectability threshold and high reliability to characterize damage in aerospace composite structural components to comply with the damage-tolerance requirement of the industry. Thus, the objectives of this research are two-fold: (i) propose ML classification algorithms that can estimate the damage severity of composite laminates in the presence of matrix cracks, and (ii) propose ML regression algorithms that can characterize, with high accuracy, delamination and matrix cracking damage.

After solving the ERT problem of composite laminates with different delamination and matrix cracking damage scenarios, ML algorithms were trained based on electrical resistance measurements taken at the boundary electrodes. The methods studied include NN, KNN, SVM, and RF, and the goal is to compare the predictive capability of these algorithms in terms of spatial resolution and accuracy. The main contribution of this work is that it explores the integration of the ERT NDE method with several well-known machine learning algorithms to identify, classify, and characterize delamination and matrix cracking damage in composites. The obtained accuracy of the proposed ML algorithms to detect and classify these independent damage modes was up to 95%, outperforming previous similar studies in which Kriging surrogate models were implemented [35]. To the best of our knowledge, no other article in the literature has reported a similar evaluation before.

The rest of the document is organized as follows. Section 2 introduces the governing equations of the ERT method applied to composites. In Section 3 the machine learning algorithms used in this work are briefly introduced. Section 4 provides a detailed discussion on the use of the ML to classify and characterize damage. The results are discussed in Section 5. Finally, the conclusions are presented in Section 6.

2. Electrical Resistance Tomography for Structural Health Monitoring of Composites

CFRP composites have anisotropic electrical conductivity properties. These materials are highly conductive in the fiber direction, but in the in-plane transverse-to-fiber and normal-to-plane directions, the conductivity is two and three orders of magnitude smaller, respectively. For this reason, the anisotropic conductivity tensor Σ of any ply in a laminate can be expressed as follows:

$$\Sigma = \begin{bmatrix} \Sigma_1 & 0 & 0 \\ 0 & \Sigma_2 & 0 \\ 0 & 0 & \Sigma_3 \end{bmatrix}, \tag{1}$$

where Σ_1 is the conductivity along the fiber direction, Σ_2 is the in-plane transverse-to-fiber direction conductivity, and Σ_3 is the normal-to-plane direction conductivity. Damage in the form of delamination and matrix cracking in composites increases the resistivity of each of the plies as the electrical current flow changes its path to the adjacent plies to get around the cracks. These changes in the current path lead to changes in the global potential field, which can be captured from electrical resistance or voltage measurements taken at the surface electrodes.

Matrix cracking damage affects mainly the resistivity ρ_2 and ρ_3 of the laminate. After undergoing damage, the homogenized effective resistivity ρ_2^* of the laminate can be expressed as follows [35]:

$$\rho_2^* = (1 - d)\rho_2, \tag{2}$$

where $\rho_2 = 1/\Sigma_2$ is the normal-to-fibre resistivity of the undamaged ply. The mesoscale damage parameter d represents the matrix cracking density of a ply in the composite, where typical values of d range in between $0 \le d \le 0.8$ [36].

To capture the effect of the matrix cracking mode on the overall potential field relative to the sensing electrodes, the resistance change due to transverse ply cracking is expressed by the moments of the resistance change. The first four integrated resistivity moments M_q, for $q = 1 - 4$, of a composite laminate with respect to a reference axis located at z_0 are as follows:

$$M_q = \sum_{k=1}^{p} \int_{z_0}^{z_k} \left(\rho_{2_{(k)}}^*\right) z^q \mathrm{d}z, \tag{3}$$

where k is the number of transverse plies in a p-ply laminate, and z is the through-the-thickness position along the ply cross-section. The lower limit of the integral is $z_0 = 0$, while the upper limit z_k represents the z-coordinate of the lower surface of each layer k.

The governing equations describing the electrical behavior of a material with a conductivity field over a domain and the associated boundary conditions are given by the following equations [8, 37]:

$$-\nabla \cdot (\Sigma \nabla u) = 0, \overline{x} \in \Omega, \tag{4}$$

$$\int_{e_l} \Sigma \frac{\partial u}{\partial \overline{n}} dS = I_l, l = 1, 2, \ldots, L, \tag{5a}$$

$$\Sigma \frac{\partial u}{\partial \overline{n}} = 0, \quad \overline{x} \in \partial\Omega \backslash U_{l=1}^{L} \quad e_l, \tag{5b}$$

$$u + \xi\Sigma \frac{\partial u}{\partial \overline{n}} = U_l, \overline{x} \in e_l, l = 1, 2, \ldots, L, \tag{5c}$$

where $\Sigma(\overline{x})$ is the anisotropic conductivity tensor that describes the spatial variations of the electrical conductivity,

and $u(\overline{x})$ the electric potential inside the body Ω measured at the lth electrode.

The first boundary condition, equation (5a), implies that the injected current I_l at each electrode must be equal to the integrated current density over that electrode e_l. The second boundary condition, equation (5b) indicates that currents are zero at the boundary where electrodes are not present. Finally, equation (5c) postulates that if perfect electric contact between the electrode and the body Ω is assumed, the contact resistance ξ term is neglected and the electrical potential u inside the body equals U_l, the electric potential under the electrode e_l.

Equations (4)–(5c) are often referred to as the forward problem in ERT. To identify and characterize damage, the inverse problem must be formulated. The inverse problem aims to find the in-plane conductivity change of the domain which relates the predamage voltages to the postdamage voltages [14]:

$$d\Sigma^* = \min_{d\Sigma} \left(\left\| dV - d\widehat{V} \right\|^2 + \left\| \lambda L d\Sigma \right\|^2 \right), \tag{6}$$

where $\mathrm{d}V(\Sigma)$ is the change in the experimental voltage measurements due to the change in conductivity distribution $\mathrm{d}\Sigma$ expressed between a reference and future states, and $\mathrm{d}\widehat{V}(\Sigma)$ the model-predicted voltage changes corresponding to a $\mathrm{d}\Sigma$ change. Since the inverse problem is severely ill-posed, regularization schemes are generally included. The generalized Tikhonov regularization [38] is the simplest and most common technique for tackling the ill-conditioning problem. The parameter λ and the regularization matrix L in equation (6) above are typically heuristically defined by the users to achieve a good trade-off between the fitted experimental data and the inherent noise of the signals. The need of regularization in equation (6) is one of the current challenges of the ERT inverse problems applied to the inverse identification of damage in composite laminates, as it requires a priori knowledge of each composite laminate.

To reduce the computational cost associated with the solution of the inverse problem in ERT, ML algorithms can be used to identify damage descriptors in composite laminates directly. These algorithms can be trained based on electrical resistance measurements of composites in the presence of damage and can then characterize the damage signatures given any potential boundary field. The use of ML tools addresses some of the current challenges of the ERT method applied to composites, which includes the need for regularization, the anisotropic electrical conductivity properties, and the ill-conditioned nature of the inverse problem.

3. Machine Learning Methods for Damage Identification and Classification in Composites

Different ML techniques are evaluated in this work to describe the electrical response of composite laminates in the presence of delamination and matrix cracking damage. These algorithms are used along with the ERT method to: (1) classify the damage severity of delamination cracks; (2) for a given damage state, predict the electrical resistance variations at the boundaries of the composite; and (3) for an unknown damage state, characterize the delamination damage shaping parameters and homogenized matrix cracking saturation level.

The first problem requires the development of classification ML algorithms for estimating the damage severity of composites. In this work, damage severity is defined in terms of the delamination crack size x_1. Following the study by Kumar and Rai [39] in which composite laminates were subjected to different levels of impact energy to create delamination, three classes are defined herein: damage severity class 1 ($5\,\mathrm{mm} < x_1 \le 10\,\mathrm{mm}$), damage severity class 2 ($10\,\mathrm{mm} < x_1 \le 20\,\mathrm{mm}$), and damage severity class 3 ($20\,\mathrm{mm} < x_1 \le 30\,\mathrm{mm}$).

The second problem requires the development of regression ML algorithms for predicting the electrical resistance variations of the composite in the presence of damage, assuming a set of damage parameters that include delamination size, location, and resistivity moments that represent the matrix cracking damage state. This problem will allow us to assess the accuracy of the regression ML algorithms that will then be used for characterizing damage.

The last problem requires predicting the delamination descriptors (size and location) and the resistivity moments associated with matrix damage, given the electrical resistance measurements at different combinations of surface electrodes. We compare different ML techniques to investigate which method will result in the most accurate estimations of the damage state in the composite. Descriptions of the ML techniques evaluated in this work are described next.

3.1. Neural Networks. Neural networks (NN) architectures are capable of representing complex functions by nonlinear learned transformations [40]. NNs are machine learning algorithms inspired by the human brain and composed of artificial neurons. Each neuron is represented by activation units $\{a_j\}$, arranged in multiple layers: the input layer $X = \{x_i \mid i = 1, 2, \ldots, N\}$, where N is the number of inputs; the output layer $\widehat{Y} = \{\widehat{y}_i \mid i = 1, 2, \ldots, M\}$, where M is the number of outputs; and the hidden layers $Z = \left\{z_i^{(l)} \mid l = 1, 2, \ldots, L, i = 1, 2, \ldots, K\right\}$, where L is the number of hidden layers and K represents the number of hidden units in the l_{th} layer.

Each hidden layer $z^{(l)}$ of the network is defined by equations (7) and (8) as the linear combinations of the hidden units of the previous layer $\left\{z_i^{(l-1)}\right\}$, followed by a nonlinear activation function $h(\cdot)$ as follows [41]:

$$a_i^{(l)} = \sum_{j=1}^{K} w_{ij}^{(l)} z_i^{(l-1)} + b_i^{(l)}, \tag{7}$$

$$z_j^{(l)} = h\left(a_j^{(l)}\right), \tag{8}$$

where $w_{ij}^{(l)}$ and $b_i^{(l)}$ represent the weights and biases parameters to the corresponding l_{th} layer, respectively. If $(l-1)$ is the input layer, than $z^{(0)} = X$.

In order to train the network, it is necessary to define a loss function $L(\widehat{Y}, Y)$ associated with each supervised example (x_i, y_i), where $Y = \{y_i \mid i = 1, 2, \ldots, M\}$ represents the corresponding real values or labels. The goal is to obtain a global minimum of the loss function by using different optimization methods [40]. Table 1 shows common hyper-parameters values generally chosen for NN training.

3.2. Support Vector Machine. The support vector machine (SVM) is a supervised nonprobabilistic binary machine learning technique proposed by Cortes and Vapnik [42] used in classification and regression problems. Among the advantages of SVM are that it works well with a small number of features, is robust against the models' errors, and is computationally efficient compared to other ML algorithms. The SVM algorithm uses training data to determine the best decision boundary that separates an n-dimensional space into classes. When new data is classified, the decision boundary is used to assign it to the correct category. The decision boundary is called a hyperplane. The SVM algorithm transforms input vectors into a higher-dimensional feature space, where a hyperplane is constructed for easier class separation. The optimal hyperplane is built for the two-class classification problem by maximizing the distance (margin) between data from both classes, becoming an optimization problem. Nonlinear kernel functions perform high-dimensional feature space transformation to maximize the hyperplane margin [43]. Thus, the selection of the kernel function has an important impact on the SVM performance. Additionally, the C parameter, which controls the trade-off between margin maximization and training error minimization, should be carefully selected [43]. As the value of C is increased, the distance between the boundaries of the two classes is reduced. The multiclass problem is decomposed into multiple binary subproblems and applied using the same principle utilizing the one-vs-one or one-vs-all approach for multiclass classification. The SVM algorithm yields excellent performance when there is a clear separation margin between classes. Also, it is memory efficient in many cases. On the contrary, the algorithms do not perform well when the data set is large or when the data instances are not well separated, i.e., when they overlap. Table 2 shows common hyper-parameters values generally chosen for SVM training.

3.3. Random Forest. Random forest (RF) [44] is a supervised ensemble learning technique for classification and regression based on decision trees (DT). A DT is a technique for decision support that uses a tree structure. A DT has three elements: decision nodes, leaf nodes, and root nodes. The DT algorithm divides data from the training set into branches in the decision process until the algorithm attains a leaf node. These nodes represent attributes that are used for predicting the outcome. DT shows some disadvantages, such as bias and overfitting. To provide better performance than the DT algorithm, RF uses multiple DT. Each DT is constructed by randomly selecting data from the training set, using a method known as bagging [45]. The bagging procedure selects a random sample of data in the training set with replacement; i.e., individual data points can be chosen more than once. The models built with the data samples are trained independently, and the algorithm makes the classification decision based on the class that was chosen by the majority of DT, improving the prediction accuracy [45]. The main advantages of RF over DT are the reduced risk of overfitting and handling large datasets efficiently. In contrast, it consumes more time and requires more computational resources than the DT algorithm. The value of the hypermeters in RF impacts the predictive power and speed of the model. Table 3 shows common hyper-parameters values generally chosen for RF training.

3.4. K-Nearest Neighbor. The k-nearest neighbor (kNN) [46] is a nonparametric learning technique used for classification and regression tasks. The KNN algorithm compares a given test data with the training data to find which is similar in order to classify it [47]. Data used by the KNN algorithm is a point in an n-dimensional space. Thereby, all the training sets are stored in n-dimensional pattern space. To classify a new instance using the KNN algorithm, it searches for the n-dimensional space for the k training instances closest to the given input. A distance metric, such as the Euclidian distance, is used to define the proximity of the specified input and training instances. The algorithm classifies a given input instance as the most common class among its k neighbors. When a new data instance is classified, its distance from the labeled object is calculated. Afterward, the number of nearest neighbors is specified. Lastly, the class classified by most of the k of nearest neighbors is allocated as the label to the given instance. The main advantages of KNN are that it is simple to implement and that there is no need to build a model to use it. However, it can perform slowly as the number of data instances grow. Among the most important hyper-parameters of the KNN algorithm are the distance function and the value of k. Table 4 shows common hyper-parameters values generally chosen for KNN training.

The ML algorithms reviewed in this section have been used successfully to address multiple classification and regression problems. Since these algorithms use different strategies to address the classification and regression problems, their results may differ depending on the nature of each situation. Due to their excellent, proven performance, we chose to explore their provided accuracy in the context of SHM and CFRP applications.

4. Application of Machine Learning Techniques for Damage Classification and Characterization in Composite Laminates

This section provides detailed information regarding the use of the supervised ML algorithms employed to classify and characterize damage in composite laminates using ERT.

4.1. Generation of Synthetic Data. The finite element method was used to simulate the electrical resistance variations of composite laminates in the presence of matrix cracking and

Table 1: Neural network hyper-parameter values.

Hyper-parameter	Description	Selection
Hidden layers	Number of hidden layers in the network.	1, 2, 3
Activation units	Number of activation units in each layer.	8, 16, 32, 48, 64, 128
Activation function	Defines the output of the activation units.	ReLU, softmax, sigmoid, tanh, LeakyReLU
Optimizer	Loss function optimization model.	SGD, Adam, RMSprop
Learning rate	The amount that the weights are updated during training.	0.1, 0.01, 0.001, 0.0001
Batch size	Number of samples used for each weight update iteration.	1, 16, 32, 64

Table 2: Support vector machine hyper-parameter values.

Hyper-parameter	Description	Selection
C value	Controls the trade-off between margin maximization and training error minimization. As the C value increases, the error tends to increase.	0.01, 0.1, 1, 10, 100, 1000
Kernel	Maps inputs into a higher-dimensional feature space.	Linear, polynomial, radial, sigmoid
Gamma	Gamma value is a kernel variable. Controls the influence of farest samples in the construction of the boundary decision. As the gamma value increases, the model tends to overfit.	0.0001, 0.001, 0.01, 0.1, 1, 10

Table 3: Random forest hyper-parameter values.

Hyper-parameter	Description	Selection
N_estimators	Number of trees.	30, 50, 100, 300
Criterion	Function to measure the split quality.	Gini, entropy, mse
Max_depth	Maximum depth of the tree.	10, 30, 50, 100
Min_samples_leaf	Minimum number of samples required to be a leaf node.	3, 5, 10, 30
Max_features	Number of features considered for best split.	None, auto, sqrt, log2
Bootstrap	Random sampling with replacement.	True, false

Table 4: K-nearest neighbor hyper-parameter values.

Hyper-parameter	Description	Selection
N_neighbors	Number of neighbors.	1, 3, 5, 10, 15, 30, 50
Algorithm	Nearest neighbors algorithm implementation.	Auto, ball_tree, kd_tree, brute
Leaf_size	Leaf size passed to BallTree or KDTree.	1, 3, 10, 30, 50
Metric	Distance metric.	Euclidean, Manhattan, Minkowski

delamination by solving the forward problem outlined in Section 2. A 2D Finite Element (FE) model of a 16-ply laminate with 14 equally spaced surface electrodes was considered. The commercial software ANSYS Parametric Design Language (APDL) Mechanical 15 was used to solve the problem. Carbon-epoxy composite laminates of two different stacking sequences were analyzed: $(0_4/90_4)_s$ and $[(0/90)_4]_s$. While the later stacking sequence is representative of thick composite laminates, the first stacking sequence is used to study the electrical response of thin laminates. However, for consistency in the analysis, the number of plies of same orientation in the $(0_4/90_4)_s$ laminate was increased to match the thickness of the $[(0/90)_4]_s$ laminate. In both cases, anisotropic electrical conductivity properties corresponding to a fiber volume fraction of 62% were used. The surface electrodes were modeled as thin silver films, and isotropic conductivity properties were considered.

Eight-node quadrilateral planar elements (PLANE 230) of element size 0.125 mm were used, which resulted in one element through the thickness of each ply. Delamination damage was simulated by introducing doubly defined nodes at regions of the crack surface and by altering the connectivity of these nodes. Current and voltage were injected and measured at the same pair of electrodes, following the two-probe method in ERT. A schematic of the 2D FE model of the composite laminate can be observed in Figure 2. The reader is referred to Diaz-Montiel et al. [35] for more information on the details of the FE modeling.

The FE model was used to simulate the electrical behavior of composite laminates in the presence of delamination and matrix cracking damage. Since a 2D FE model is used, the matrix cracking damage mode only affects the resistivity ρ_2 of the 90° transverse plies. Design space of damage cases was sampled from a Latin Hypercube

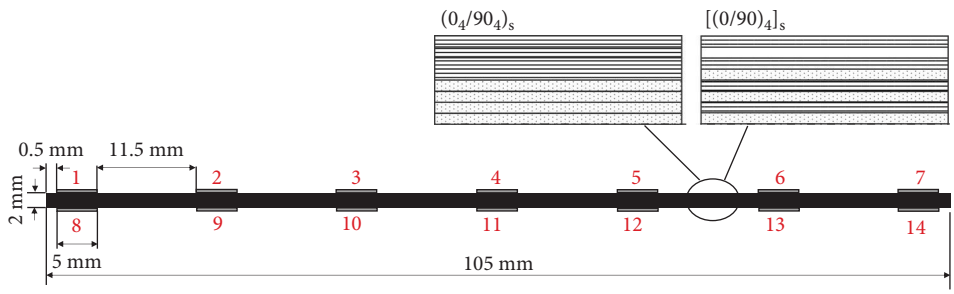

FIGURE 2: Schematic of the composite laminate model with surface electrodes used in the FE simulations to measure electrical resistance values. The two laminate stacking sequences considered in this work are also depicted.

Sampling (LHS) design of 990 points to train the machine learning algorithms. The obtained synthetic data is structured in a matrix of resistance values $\mathbf{R}$, in which each row represents a damage case in the composite and each column the electrode combination at which resistance was measured. Thus, the matrix takes the form as follows:

$$\mathbf{R} = \begin{bmatrix} \mathbf{r}_{1,1} & \cdots & \mathbf{r}_{1,j} & \cdots & \mathbf{r}_{1,M} \\ \vdots & \vdots & \vdots & & \\ \mathbf{r}_{i,1} & \cdots & \mathbf{r}_{i,j} & \cdots & \mathbf{r}_{i,M} \\ \vdots & \vdots & \vdots & & \\ \mathbf{r}_{N,1} & \cdots & \mathbf{r}_{N,j} & \cdots & \mathbf{r}_{N,M} \end{bmatrix}, \tag{9}$$

where M is the number of observations, and N is the number of damage cases. Since a total of $n_e = 14$ electrodes are considered, the possible number of electrode pair combinations to serve as injection/measurement sites results in $C(n_e, 2) = 91$. An additional set of 100 test points sampled from an LHS design was generated to assess the accuracy of the trained algorithms.

4.1.1. Data Normalization. Data normalization is a common preprocessing approach to make features contribute equally to the model. The performance of distance-based machine learning algorithms such as NN, SVM, and KNN, are commonly affected by the range of feature values. There exist several feature normalization methods that transform raw data into a particular range of values [48]. In this work, we utilized two of the most common methods for data normalization [48]:

(i) Min-Max normalization: scales and translates data to a given range $[R\min, R\max]$ by:

$$[\mathbf{x}_i]_{\text{MinMaxNorm}} = \frac{\mathbf{x}_i - \min(\mathbf{x}_i)}{\max(\mathbf{x}_i) - \min(\mathbf{x}_i)} (R\max - R\min) + R\min, \tag{10}$$

where $\mathbf{x}_i$ denotes an instance of the data, and $\min(\cdot)$ and $\max(\cdot)$ denotes the minimum and maximum value of the i_{th} feature, respectively. For our experiments, we considered a feature range of $[R\min, R\max] = [0, 1]$.

(ii) Standard normalization (or z-score normalization): scales features using the mean and standard deviation data measures, resulting in values centered around the mean with a unit standard deviation. Standard normalization is represented by the equation (11) as follows:

$$[\mathbf{x}_i]_{\text{StdNorm}} = \frac{\mathbf{x}_i - \mu_i}{\sigma_i}, \tag{11}$$

where μ_i and σ_i denote the mean and standard deviation of the i_{th} feature, respectively.

Standard normalization can be helpful when data follows a Gaussian distribution. However, there is no specific rule for choosing a normalization approach, and it will depend on data and machine learning techniques. For our experiments, electrical resistance responses were scaled using standard normalization, while damage size, location, and matrix cracking damage values were scaled using min-max normalization.

4.1.2. Multiplicative Gaussian Noise Simulation. One of the limitations of the ERT method is its high sensitivity to noise. This noise is often a result of uncertainties in the current injection and/or voltage measurement processes. Although the finite element mesh introduces discretization errors due to slight bias and interpolation errors, we also wanted to assess the robustness of the proposed ML models when different noise levels were added to the data.

Multiplicative noise is used since voltages and electrical resistance values are linearly proportional to each other ($V = RI$) under a fixed electrical current. Therefore, the electrical resistance uncertainties will result in a proportional rise in the voltage measurements uncertainties [26]. A zero-mean multiplicative Gaussian noise was added to the electrical resistance test data (100 LHS points) as follows.

Let $\mathbf{r}_i$ be the i_{th} electrical resistance signal compromising the 91 electrode combinations responses. Let n_{ij} be a

realization of zero-mean Gaussian distribution $\mathcal{N}(0, \sigma^2)$ where σ^2 denotes the noise distribution variance. The noisy electrical signal values, $\mathbf{r}_{ij}^*$, are modeled by equation (12) as follows [26]:

$$\mathbf{r}_{ij}^* = \mathbf{r}_{ij}\left(1 + n_{ij}\right), \text{with } n_{ij} \sim \mathcal{N}\left(0, \sigma^2\right), \tag{12}$$

where n_{ij} values are assumed to be identically and independently distributed. Therefore, for small σ^2 values, n_{ij} values will be closer to zero and $\mathbf{r}_{ij}^* = \mathbf{r}_{ij}(1 + n_{ij}) \approx \mathbf{r}_{ij}$. Figure 3 shows an example of electrical resistance signals subjected to different levels of noise distributions and scaled by standard normalization.

4.2. Hyper-Parameters Selection. There are two types of parameters in machine learning models: the model parameters, which are learned directly from the data, and the model hyper-parameters, which are used to control the learning process. The task of selecting the optimal hyper-parameters values for a model is known as hyper-parameter tuning. Determining the optimal hyper-parameters values is crucial to achieving a high ML model performance [49]. There are different strategies for hyper-parameter tuning. We utilized the most commonly used grid-search strategy for traditional ML techniques, which consists of selecting different hyper-parameters values and trying all the possible configurations. Grid-search was done utilizing the GridSearchCV function from the Scikit-learn Python library [50]. For NN architectures, we used the Hyperas library [51] which is based on Bayesian optimization [52]. Tables 1–4 show the values considered for each ML model for hyper-parameter tuning. For a more detailed hyper-parameter explanation, the reader is referred to [40, 43, 45, 47, 52].

4.3. Training. Let $\mathbf{r}_\Omega$ (see Section 4.1) be the set of electrical resistance variations inside the composite laminate Ω, measured at the *ij*th electrode combination. Let $\mathbf{x}_\Omega = (x_1, x_2, x_3, x_4, x_5, x_6, x_7)$ be the vector descriptor containing the cracking size (x_1), the horizontal (x_2) and vertical (x_3) delamination location, and the conductivity moments (x_4, x_5, x_6, x_7) inside the material Ω. A description of the range of these variables in the design space is listed in Table 5.

For damage severity classification from electrical resistance responses $(\mathbf{r}_\Omega)$, it was necessary to group the cracking damages presented in composite materials and label them according to the damage size (see Section 3). This grouping produced three different classes: class 1 (198 points), class 2 (396 points), and class 3 (396 points). Then, for each evaluated model, hyper-parameter tuning was carried out (see Section 4.2), resulting in the best hyper-parameter configuration as shown in Table 6. After hyper-parameter tuning, the proposed models were trained and validated using the fitting (990 LHS) points under a 10-fold cross-validation approach [53]. Once the models had been trained, the fitted models were evaluated using the test (100 LHS) points set. After hyper-parameter tuning, the best hyper-parameter configuration is selected and evaluated using 10-fold cross-validation. The best hyper-parameters for each ML model are presented in Tables 6–8.

The next experiment seeks to predict the electrical resistance responses $(\mathbf{r}_\Omega)$ of the composite (Ω) given the damage size, location, and matrix cracking damage $(\mathbf{x}_\Omega)$ inside the material. First, hyper-parameter tuning was carried out for each ML model. Table 7 shows the best resulting hyper-parameter tuning configuration. Then, we trained and validated the ML techniques using the fitting (900 LHS) points under a 10-fold cross-validation approach. The best models resulting from cross-validation were evaluated using the test (100 LHS) points set.

Finally, the third problem consists of the inverse identification of delamination damage shaping descriptors and conductivity moments associated with matrix cracking $(\mathbf{x}_\Omega)$ given the composite electrical resistance values $(\mathbf{r}_\Omega)$. As in the previous experiments, hyper-parameter tuning was carried out to obtain the best values configuration, which is presented in Table 8. The machine learning techniques were also trained and validated using the fitting (900 LHS) points under a 10-fold cross-validation approach. Then, the best models resulting from cross-validation were evaluated using the test (100 LHS) points set.

4.4. Evaluation Metrics. For the evaluation of severity damage classifiers, the ML performance results are presented in terms of precision, recall, accuracy, misclassification error, and the area under the receiver operating characteristic (AUC-ROC) metrics [54].

The precision and recall metrics describe the per-class classification performance. The precision value indicates how many of the class predictions are true, while recall indicates how many true classes are predicted correctly. The accuracy score indicates the number of correct predictions out of the total cases, while the misclassification rate indicates the number of incorrect predictions. Equations (12)–(15) describe precision, recall, accuracy, and misclassification error metrics as follows:

$$\text{Precision} = \frac{\text{TP}}{\text{TP} + \text{FP}}, \tag{13}$$

$$\text{Recall} = \frac{\text{TP}}{\text{TP} + \text{FN}}, \tag{14}$$

$$\text{Accuracy} = \frac{\text{TP} + \text{TN}}{\text{TP} + \text{TN} + \text{FP} + \text{FN}}, \tag{15}$$

$$\text{Misclassification Rate} = \frac{\text{FP} + \text{FN}}{\text{TP} + \text{TN} + \text{FP} + \text{FN}}, \tag{16}$$

where true positives (TP) and true negatives (TN) refer to the cases where the model predicted the class correctly. In contrast, false positives (FP) and false negatives (FN) are the opposite cases; i.e., the model did not accurately predict the class. The AUC-ROC represents a trade-off between TP and FP rates under different probability thresholds for the predictive model. The AUC-ROC score represents a measure of separability; i.e., the higher the AUC-ROC values, the

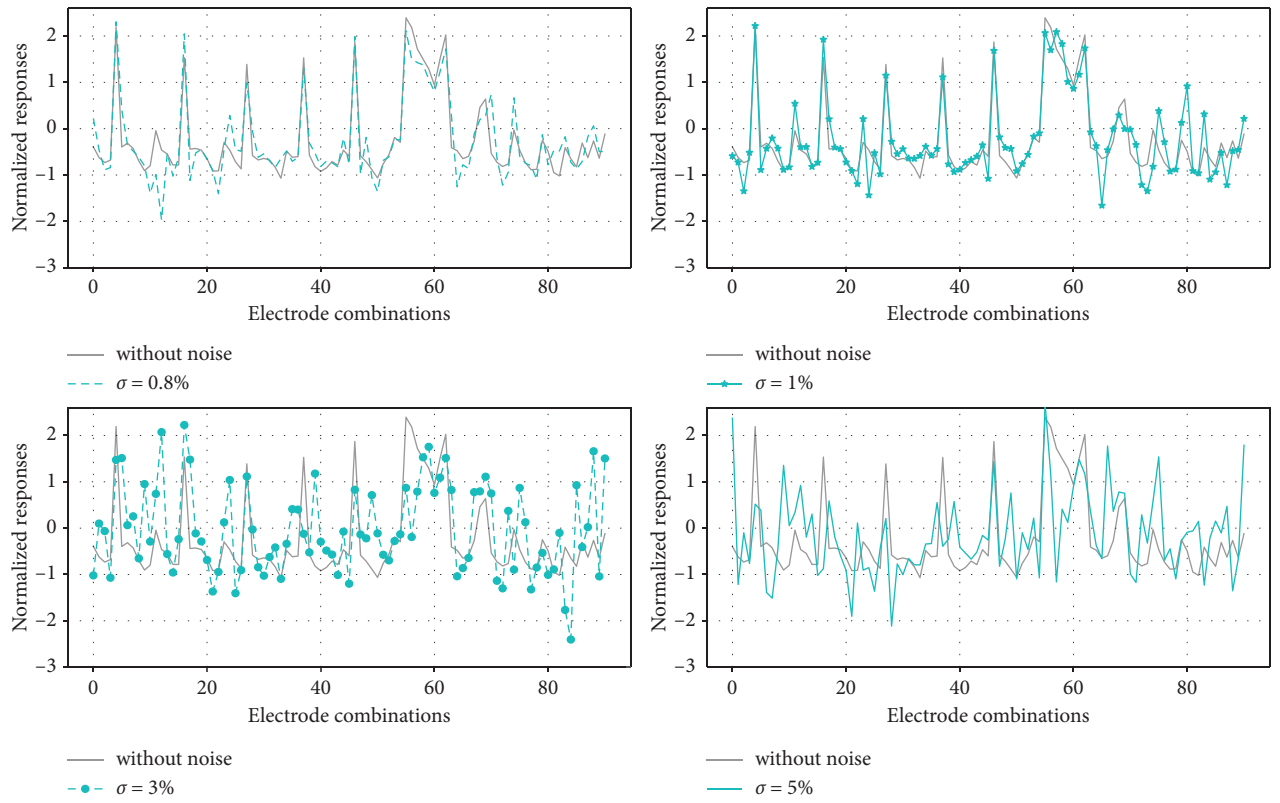

Figure 3: Example of electrical resistance signals corrupted by zero-mean multiplicative noise with different noise variance σ values and scaled by standard normalization.

Table 5: Description and range of the variables used to represent delamination and matrix cracking damage.

Design variable	Lower limit $(0_4/90_4)_a$	Upper limit $[(0/90)_4]_a$	Units
Delamination size x_1	(5–30)	(5–30)	(mm)
Delamination horizontal location x_2	(4.5–83)	(4.5–83)	(mm)
Delamination vertical location x_3	(2–15)	(2–15)	Interlaminar
First resistivity moment x_4	$0.98 - 2.94 \times 10^7$	$0.98 - 2.94 \times 10^7$	$[(\Omega \cdot \text{mm}) \cdot \text{mm}^2]$
Second resistivity moment x_5	$1.31 - 3.43 \times 10^7$	$1.31 - 3.8 \times 10^7$	$[(\Omega \cdot \text{mm}) \cdot \text{mm}^3]$
Third resistivity moment x_6	$1.96 - 4.41 \times 10^7$	$1.96 - 5.51 \times 10^7$	$[(\Omega \cdot \text{mm}) \cdot \text{mm}^4]$
Fourth resistivity moment x_7	$3.14 - 6.10 \times 10^7$	$3.14 - 8.55 \times 10^7$	$[(\Omega \cdot \text{mm}) \cdot \text{mm}^5]$

Table 6: Optimum hyper-parameters for classification of damage severity in composites.

Model	Configuration
NN	1st layer = 128, 2nd layer = 32, output layer = 3, 1st activation = tanh, 2nd activation = relu, 3rd activation = softmax, optimizer = Adam (lr = 0.01, decay = 0.01/100), batch size = 16, epochs = 100
KNN	Algorithm = auto, leaf_size = 1, metric = minkowski, n_neighbors = 1
SVM	C = 1000, gamma = 0.01, kernel = rbf
RF	Bootstrap = false, criterion = gini, max_features = sqrt, n_estimators = 300, Min_samples_leaf = 3, max_depth = none

Table 7: Optimum hyper-parameters for resistance values predictions.

Model	Configuration
NN	1st layer = 32, 2nd layer = 16, output layer = 91, 1st activation = LeakyReLU, 2nd activation = tanh, 3rd activation = LeakyReLU, optimizer = Adam (lr = 0.01, decay = 0.01/2000), batch size = 16, epochs = 2000
KNN	Algorithm = brute, leaf_size = 1, metric = minkowski, n_neighbors = 5
SVM	C = 1000, gamma = 0.1, kernel = rbf
RF	Bootstrap = true, criterion = mse, max_features = auto, n_estimators = 100, Min_samples_leaf = 3, max_depth = 50

Table 8: Optimum hyper-parameters for delamination damage and conductivity moments predictions.

Model	Configuration
NN	1st layer = 128, 2nd layer = 32, output layer = 7, 1st activation = tanh, 2nd activation = relu, 3rd activation = softmax, optimizer = adam (lr = 0.01, decay = 0.01/2000), batch size = 16, epochs = 2000
KNN	Algorithm = auto, leaf_size = 1, metric = minkowski, n_neighbors = 1
SVM	$C = 1000$, gamma = 0.01, kernel = rbf
RF	Bootstrap = false, criterion = mse, max_features = sqrt, n_estimators = 300, Min_samples_leaf = 3, max_depth = none

better the model is at distinguishing between classes. All the metrics mentioned above yield a value between 0 and 1. It is important to note that the higher the metric value, the better the model predicts.

For resistance responses and descriptor vector predictions, we utilized the following metrics to evaluate and compare the proposed ML models with the Kriging method [35, 55]. The maximum relative error (maxRE) and the maximum root-mean-square error (maxRMSE) metrics are described in equations (17) and (18), respectively, as follows:

$$\max_{i,j=1-N,M} RE = \max_j \left[\max_i \left(\frac{\mathbf{r}_{ij} - \widehat{\mathbf{r}}_{ij}}{\mathbf{r}_{ij}} \right) \right], \tag{17}$$

$$\max_{i,j=1-N,M} \text{RMSE} = \max_j \left[\frac{\sqrt{1/N \sum_{i=1}^{N} \left(\mathbf{r}_{ij} - \widehat{\mathbf{r}}_{ij} \right)^2}}{\mathbf{r}_{\mathbf{rms}}} \right], \tag{18}$$

where $\mathbf{r}$ and $\widehat{\mathbf{r}}$ describe the measured and predicted resistance responses, respectively. The RMSE metric is normalized using the root-mean-squared of the resistance values correspondent to all damage cases N at each response M with

$$\mathbf{r}_{\mathbf{rms}} = \sqrt{\frac{1}{N} \sum_{i=1}^{n} \mathbf{r}_i^2}. \tag{19}$$

The maximum cross-validation error (max CV) considers the maxRMSE of the total predictions obtained from each test set corresponding to each 10-fold cross-validation. The root-mean-squared relative error (rmsRE) defined by equation (20) as follows:

$$\text{rmsRE} = \sqrt{\frac{1}{N} \sum_{i=1}^{N} \left[\left(\frac{\mathbf{x}_i - \widehat{\mathbf{x}}_i}{\mathbf{x}_i^{ref}} \right) \times 100 \right]^2}, \tag{20}$$

where $\mathbf{x}$ and $\widehat{\mathbf{x}}$ describe the measured and predicted descriptor values, respectively, and $\mathbf{x}_i^{\text{ref}}$ represents the reference values. The relative errors for crack size (x_1) are calculated relative to the electrode center-to-center spacing. The relative errors for a crack horizontal position are calculated relative to the range of the variable x_2 used for generating the design space. The relative errors for a crack vertical position (x_3) are calculated relative to the total number of plies in the composite. Finally, the relative errors of variables x_4 to x_7 are calculated relative to the range of each of these variables. For the $(0_4/90_4)_s$ stacking sequence, the resulting reference values are $\mathbf{x}_i^{\text{ref}} = (16.5, 78.5, 16, (2.94 - 0.98) \times 10^7, (3.43 - 1.31) \times 10^7, (4.41 - 1.96) \times 10^7, (6.10 - 3.14) \times 10^7)$, and for the $[(0/90)_4]_s$ laminate, the resulting reference values are $\mathbf{x}_i^{\text{ref}} = (16.5, 78.5, 16, (2.94 - 0.98) \times 10^7, (3.8 - 1.31) \times 10^7, (5.51 - 1.96) \times 10^7, (8.55 - 3.14) \times 10^7)$.

5. Results and Discussions

5.1. Classification of Damage Severity. The damage severity classification results obtained from the 10-fold cross-validation are shown in Table 9. Results show that, for both types of composites, NN architectures successfully classified damage severity, achieving performances about 95% of accuracy and 98% of AUC-ROC for $(0_4/90_4)_s$ laminate and 94% of accuracy and 99% of AUC-ROC for $[(0/90)_4]_s$ material for the test set points. Most NN misclassified errors were presented in the second class, where damage sizes are between $(10\,\text{mm} < x_1 \leq 20\,\text{mm})$. That is because some damage sizes were too close to the limits of the classes. Figure 4 shows the classification confusion matrices of both composite materials.

Not far behind the NN performance, the SVM and RF models obtained similar performances for $[(0/90)_4]_s$ laminate, while the KNN obtained the worst evaluation results on both scenarios. These results confirmed those obtained by Schmidt [26]. However, we cannot fully compare our results with those obtained by Schmidt [26] because they performed a binary classification analysis, whereas our work is a multiclass classification analysis, i.e., the number of classes is not the same. Nevertheless, as shown in Table 9 all models achieved a high classification accuracy greater than 90%, for most cases of the two laminates considered. These results allow us to consider ML techniques as a feasible tool for classifying damage severity in composite materials.

5.2. Electrical Resistance Responses Prediction. For electrical resistance responses prediction we conducted regression analysis. Evaluated ML performances for electrical resistance response prediction for $(0_4/90_4)_s$ and $[(0/90)_4]_s$ laminates are presented in Table 10, in terms of maxCV, maxRE, and maxRMSE. The performance results of the evaluated models were compared with those obtained by the Kriging method [35]. It is important to note from Table 10 that the maxCV results from the Kriging method were computed using the leave-one-out cross-validation error, while for ML techniques, a 10-fold cross-validation approach was used. Nevertheless, the max RE and max RMSE errors were equally computed on the same test point sets for all the evaluated models.

Table 9: ML techniques results at the fitting (990 LHS) and test (100 LHS) points for damage classification.

Model	$(0_4/90_4)_s$				$[(0/90)_4]_s$			
	Fitting points		Test points		Fitting points		Test points	
	Accuracy (%)	AUC (%)	Accuracy (%)	AUC (%)	Accuracy (%)	AUC (%)	Accuracy (%)	AUC (%)
NN	94.1	99.0	95.0	98.5	94.2	99.4	94.0	99.3
KNN	90.4	92.9	90.0	93.0	83.1	87.2	89.0	92.6
SVM	93.4	98.8	95.0	98.7	93.9	99.1	94.0	99.6
RF	92.5	98.8	92.0	99.0	90.0	98.1	93.0	98.8

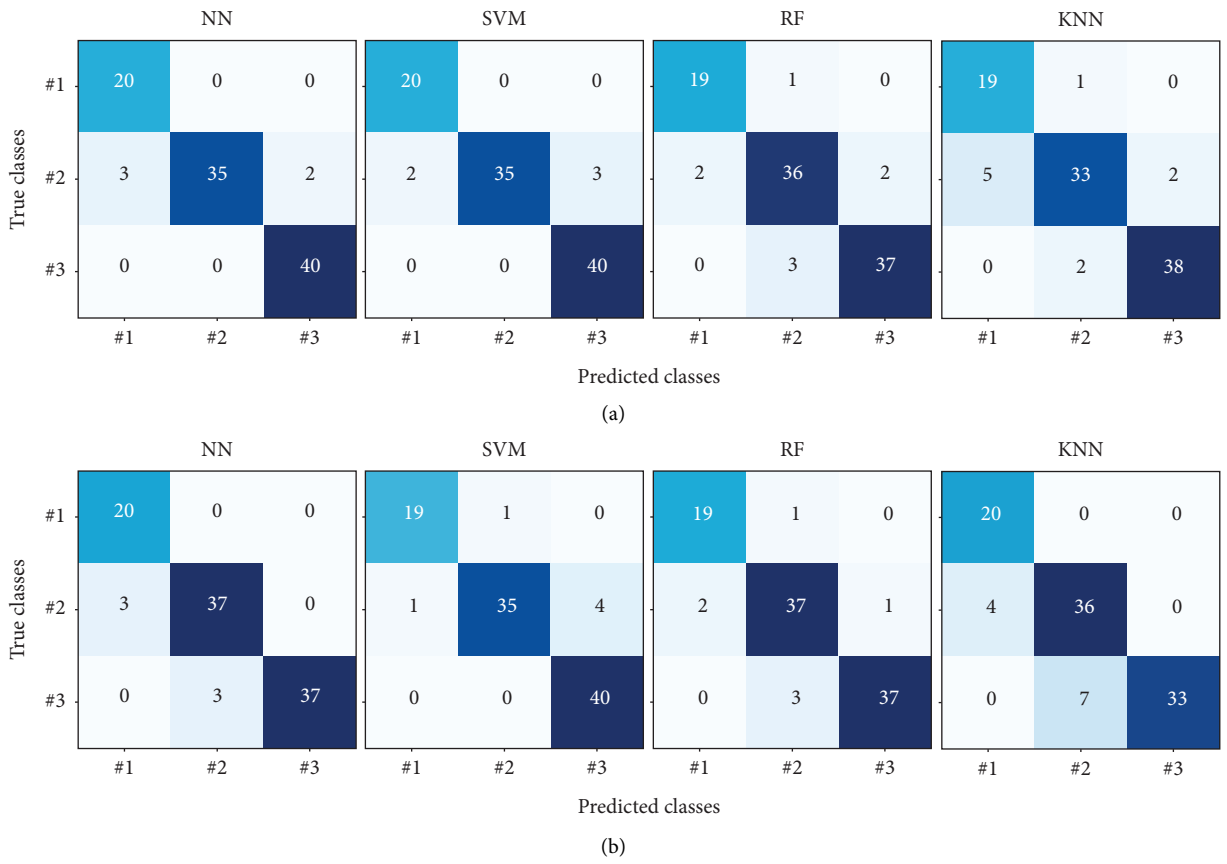

Figure 4: Confusion matrices of ML techniques for damage classification in (a) $(0_4/90_4)_s$ and (b) $[(0/90)_4]_s$ composite laminates.

Table 10: ML techniques results at the fitting (900 LHS) and test (100 LHS) points for resistance values prediction.

Model	$(0_4/90_4)_s$			$[(0/90)_4]_s$		
	Fitting points	Test points		Fitting points	Test points	
	max CV	max RE (%)	max RMSE (%)	max CV	max RE (%)	max RMSE (%)
Kriging	0.006*	39.734	15.50	0.0149*	39.777	9.281
NN	0.017	11.016	3.288	0.0326	14.927	4.422
KNN	0.063	28.694	7.153	0.0877	44.209	9.876
SVM	0.094	37.368	10.161	0.114	45.562	14.079
RF	0.030	18.499	3.260	0.0465	22.660	6.120

*max CV for kriging method is computed using leave-one-out cross-validation error.

Although the maxCV errors were lower for the Kriging method (see Table 10), its performance over the test points sets was not the best. For both types of composites $(0_4/90_4)_s$ and $[(0/90)_4]_s$, the NN architectures achieved the lowest maxRE error, about 11%, and 14%, respectively, and the maxRMSE error, about 15%, and 9%, respectively, compared to the other models. In particular, NN models achieved errors less than one-third and one-half for the $(0_4/90_4)_s$ land $[(0/90)_4]_s$ laminates, respectively, compared with those obtained by the Kriging approach.

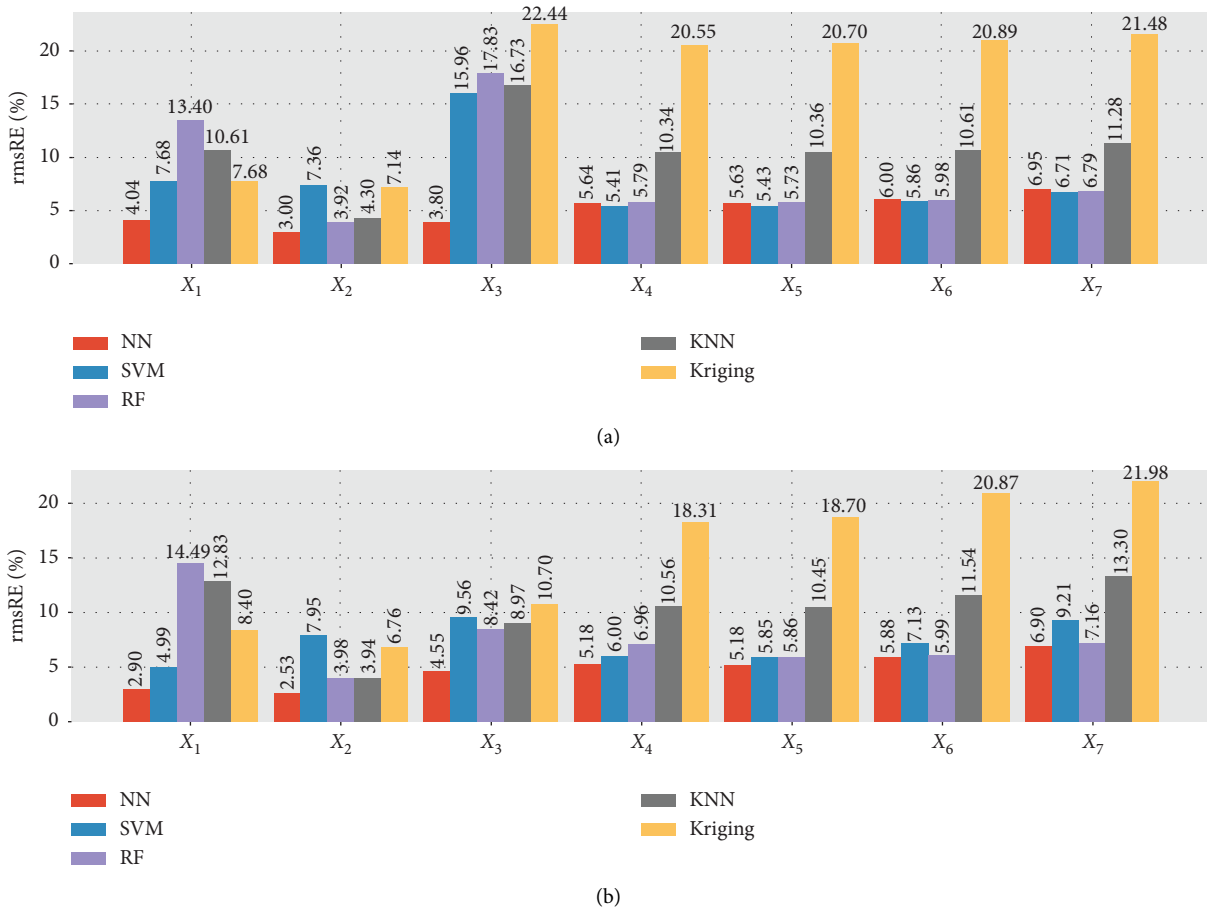

FIGURE 5: Inverse identification of delamination damage and conductivity moments for (a) $(0_4/90_4)_s$ and (b) $[(0/90)_4]_s$ laminates.

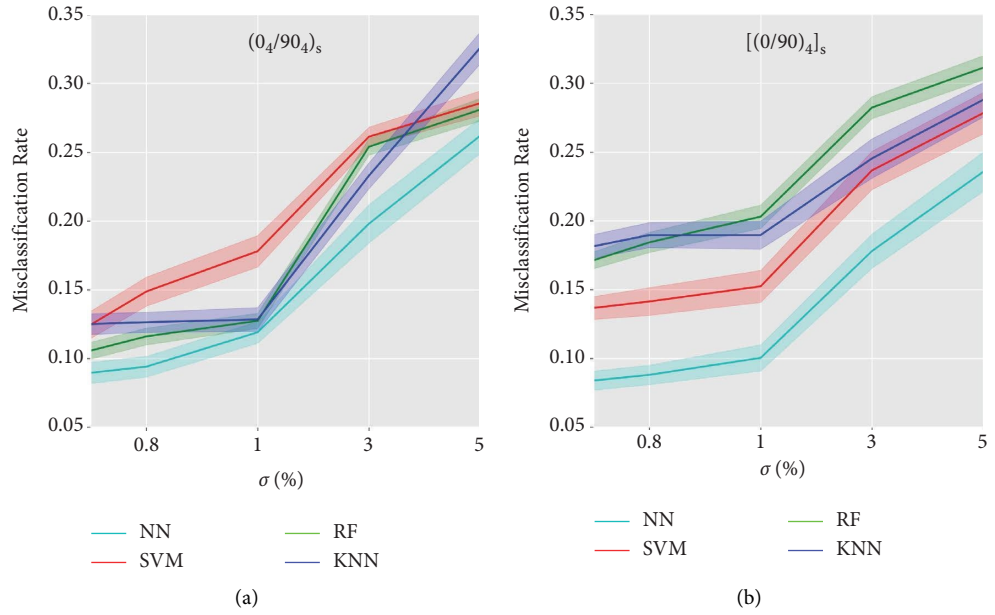

FIGURE 6: Means of damage size classification results corrupted by multiplicative gaussian noise with different standard deviation values (σ) for (a) $(0_4/90_4)_s$ and (b) $[(0/90)_4]_s$ laminates.

FIGURE 7: ML models performance results of delamination damage (x_1, x_2, x_3) and conductivity moments (x_4, x_5, x_6, x_7) prediction under different levels of multiplicative gaussian noise for $(0_4/90_4)_s$ laminate.

On the other hand, even though the RF model achieved maxRMSE errors that were not far from those obtained by the NN architectures, the maxCV and maxRMSE values were not too close. However, the RF maxRE errors are less than 23% and the maxRMSE errors are less than 7% for both scenarios. Finally, the SVM model obtained the worst performance, with maxRE values around 40% and maxRMSE errors up to 10%. We can observe that ML models can describe more accurately the electrical behavior of the $(0_4/90_4)_s$ stacking sequences, in particular NN and RF, and have achieved promising results that could be a baseline for the development of more robust ML models.

5.3. Delamination Damage and Conductivity Moments Prediction. Our last experiment consists of the prediction of cracking size, location, and conductivity moments by means of electrical resistance responses for different laminate stacking sequences, using regression methods. Performance results of machine learning and Kriging [35] models on the test points sets are summarized in Figure 5 in terms of the rmsRE. From Figure 5, it can be observed that delamination damage values and conductivity moments are successfully identified by the NN model regardless of the laminate type. The root-mean-square relative crack size and location errors for NN architectures were less than 5%,

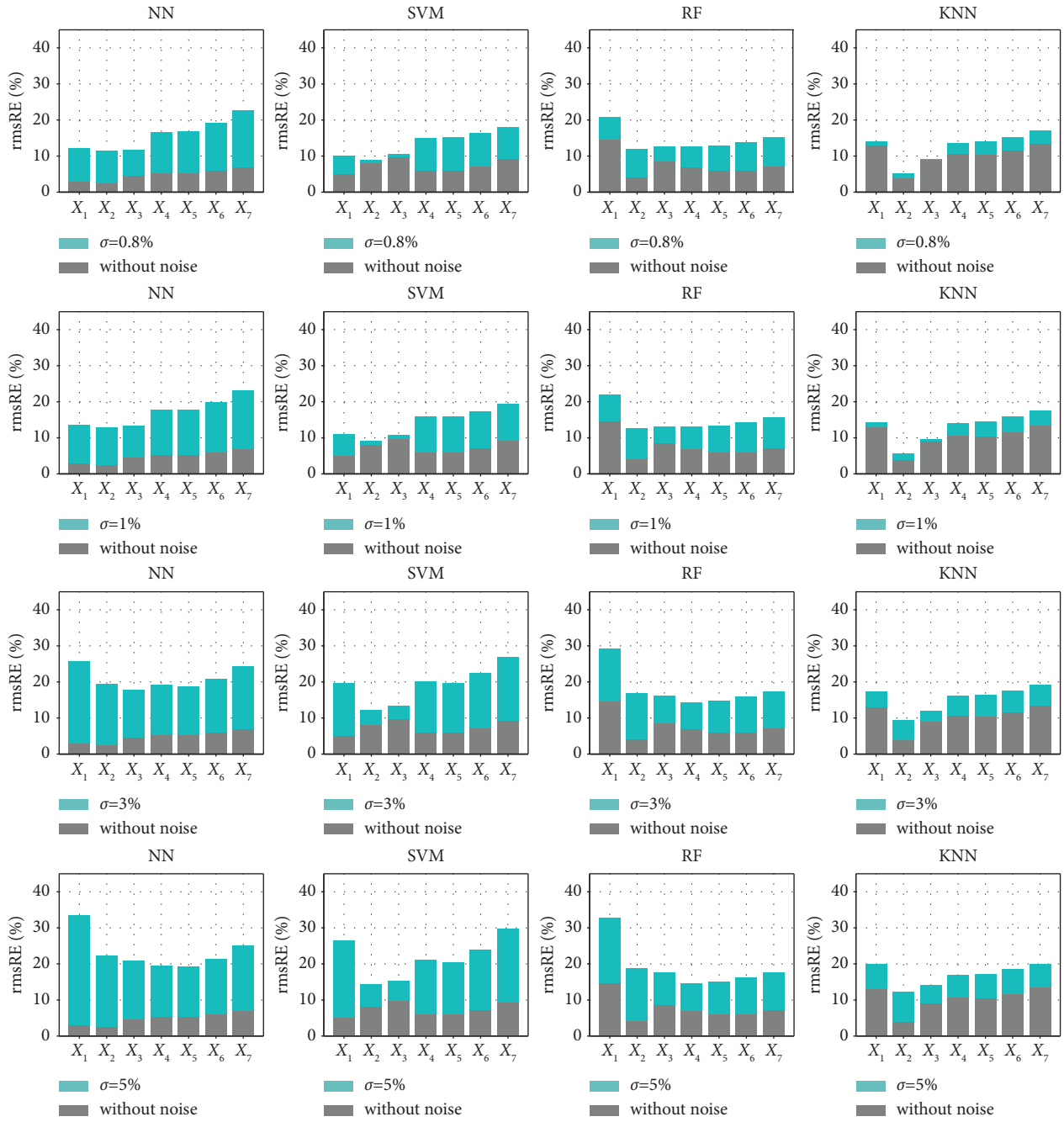

FIGURE 8: ML models performance results of delamination damage (x_1, x_2, x_3) and conductivity moments (x_4, x_5, x_6, x_7) prediction under different levels of multiplicative gaussian noise for $[(0/90)_4]_s$ laminate.

while the relative error associated with conductivity moments was around 6%. Cracking size (x_1) and vertical location of delamination (x_3) seem to be the most difficult values to predict for most models in the $(0_4/90_4)_s$ and $[(0/90)_4]_s$ composites. Furthermore, we can observe that the Kriging model completely fails in predicting conductivity moments, with relative errors around 20% for both types of the evaluated materials.

According to the evaluation results, the SVM and RF could also identify the conductivity moments associated with matrix cracking, with rmsRE values around 6%, for both types of stacking sequences. However, RF models obtained the higher errors on cracking size prediction, with a rmsRE around 14%. Besides, for the $(0_4/90_4)_s$ laminate, both models (SVM and RF) obtained errors up to 15% for the prediction of the delamination interlaminar position (x_3).

So far, NN models showed to identify the damage descriptors from electrical resistance values successfully. However, in order to verify these results, more experiments with experimental data are needed. In the following section, the simulation of noisy electrical resistance values was evaluated to analyze the robustness of the models to small perturbations in the data.

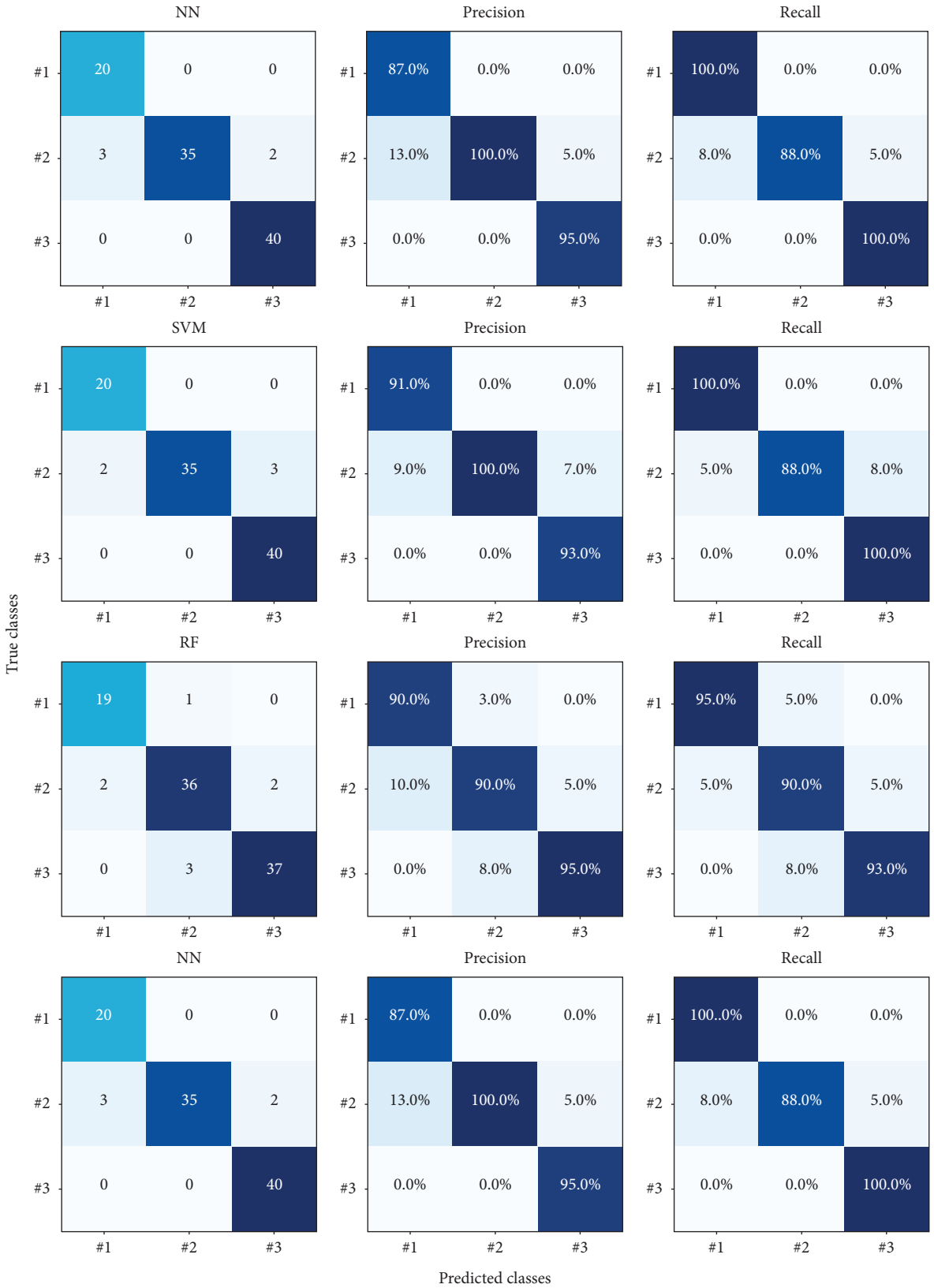

FIGURE 9: Confusion matrices of ML techniques for damage classification of $(0_4/90_4)_s$ laminates.

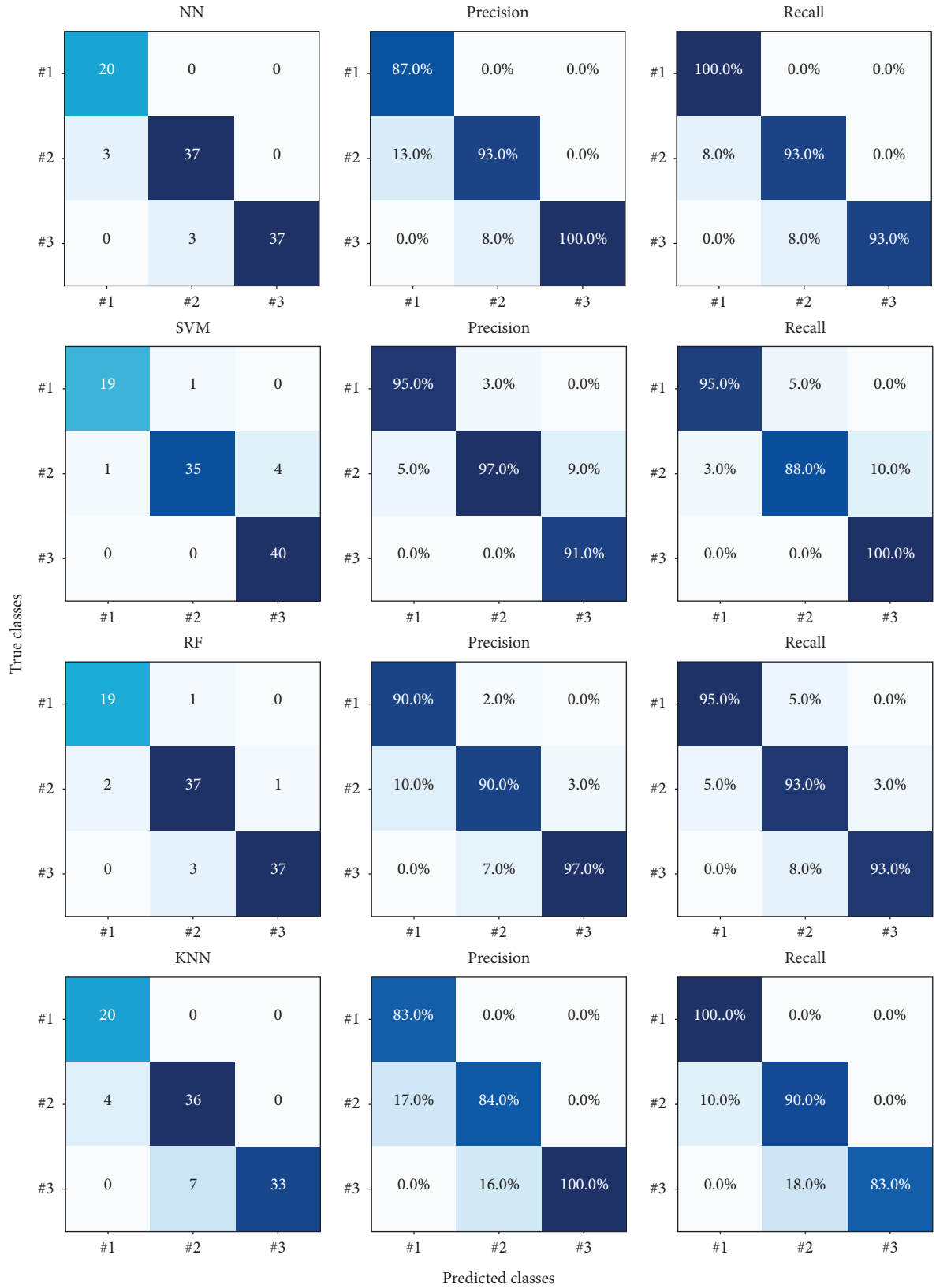

Figure 10: Confusion matrices of ML techniques for damage classification of $[(0/90)_4]_s$ laminates.

5.4. Performance of ML Models under Noise Perturbations. In order to evaluate the robustness of the ML predictors, we investigate the performance of the models assuming noise cannot be removed entirely from the measurement signals at the surface electrodes. Test set points were corrupted by multiplicative Gaussian noise (see Section 4.1.2) at different noise standard deviations (0.5%, 0.8%, 1%, 3%, and 5%) repeated 30 times. Figure 6 shows the average results for the cracking size classification problem assuming different noise standard deviations (0.5%, 0.8%, 1%, 3%, and 5%) and 95% confidence intervals (CIs).

As expected, as the standard noise deviation increases, the misclassification rate increases for all the evaluated models. From Figure 6, we can notice that, under 1% of noise standard deviation, ML models' performances keep under 15% of misclassification errors. However, with the noise above $\sigma = 1\%$, the errors increase very quickly. This error increase is not a surprising result since electrical response values corrupted by noise with standard deviations of $\sigma = 3\%$ and $\sigma = 5\%$ are significantly modified compared with the reference values (see Figure 3).

Again, NN models achieved the lowest misclassification rates compared to the other evaluated methods for both types of composites. The NN models maintained errors below 25%, except for $\sigma = 5\%$, where the error was slightly higher. On the other hand, SVM and RF obtained the worst performances for $(0_4/90_4)_s$ and $[(0/90)_4]_s$ materials, respectively.

For the problem of delamination damage and conductivity moments prediction, Figures 7 and 8 show the average results assuming different noise standard deviations (0.8%, 1%, 3%, and 5%). Although the NN architectures successfully identified the delamination damage values and conductivity moments from the electrical responses (see Figure 5), they do not seem to maintain the same behavior under different levels of noise. From Figures 7 and 8, we can observe that the root-mean-squared relative errors of NN architectures were increased more than threefold, even for low noise standard deviation values. On the other hand, KNN and RF models showed higher robustness to noise perturbations, with errors remaining below 20% in the prediction of conductivity moments and delamination damage, except for size prediction, where rmsRE increased to double for the RF model. Surprisingly, the KNN method proved to be more robust to unexpected values compared to the evaluated models.

Figure 9 shows the confusion matrices of ML techniques for damage classification of $(0_4/90_4)_s$ laminates, whereas Figure 10 shows the confusion matrices of ML techniques for damage classification of $[(0/90)_4]_s$ laminates.

6. Conclusions

This work addresses three problems related to the damage identification and characterization in composite laminates via ERT and supervised ML techniques, including NN, KNN, SVM, and RF. The proposed machine learning techniques were trained and evaluated utilizing synthetic data that simulates the electrical behavior of composite laminates in the presence of delamination and matrix cracking damage.

The first problem is classifying cracking damage severity in the composite material given a set of electrical resistance measurements. Results show that the NN and SVM models successfully classified damage severity. The NN and SVM cracking classifiers achieved a 95% and 94% of accuracy for $(0_4/90_4)_s$ and $[(0/90)_4]_s$ laminates, respectively. Besides, both models achieved AUC-ROC values up to 98% for the two types of composites.

The second problem addressed in this work is the electrical resistance responses prediction of the composite material employing delamination size, location, and conductivity moments. The ML evaluation results were favorable for the NN models. In particular, the NN models reduced almost half of the maxRE and one-third of the maxRMSE errors compared with those obtained by the Kriging method for both laminate types.

The last problem is the prediction of delamination damage (size and location) and conductivity moments through electrical resistance responses for the two types of stacking sequences. Evaluation results showed that the NN architecture successfully identified delamination damage parameters and conductivity moments, with a rmsRE of about 6%. However, KNN and RF models were more robust to noisy signals, achieving errors lower than 20%.

Evaluating the performance of ML techniques using experimental data is necessary for a more robust study. This is part of the authors' future work. However, all the evaluations presented in this work allow us to consider ML techniques as feasible tools for identifying and predicting damage in composite laminates using the ERT method. In addition, a larger dataset could also be used in the future for developing deep neural networks that could achieve more accurate predictions.

Data Availability

The dataset used in our work is available in the following link: https://www.kaggle.com/datasets/arnoldodiazramirez/damage-in-composite-laminates-using-ert.

Conflicts of Interest

The authors declare that there are no conflicts of interest.

Authors' Contributions

Julia Diaz-Escobar and Paulina Díaz-Montiel contributed equally to this study.

Acknowledgments

This work was partially supported by the Tecnológico Nacional de Mexico.

References

[1] C. A. S. Faa, "Advisory Circular (AC)," *Change*, vol. 1, pp. 20–107B, 2010.

[2] S. S. Kessler, "Certifying a structural health monitoring system: characterizing durability, reliability and longevity," in *Proceedings of the 1st International Forum on Integrated Systems Health Engineering and Management in Aerospace*, pp. 7–10, Napa, CA, USA, June 2005.

[3] I. A. T. A. Airline, *Maintenance cost executive commentary. Tech. Rep. FY2019 Data*, International Air Transport Association, Montreal, Canada, 2020.

[4] A. K. Jardine, D. Lin, and D. Banjevic, "A review on machinery diagnostics and prognostics implementing condition-based maintenance," *Mechanical Systems and Signal Processing*, vol. 20, no. 7, pp. 1483–1510, 2006.

[5] R. Schueler, S. P. Joshi, and K. Schulte, "Damage detection in CFRP by electrical conductivity mapping," *Composites Science and Technology*, vol. 61, no. 6, pp. 921–930, 2001.

[6] A. Todoroki, M. Tanaka, and Y. Shimamura, "High performance estimations of delamination of graphite/epoxy laminates with electric resistance change method," *Composites Science and Technology*, vol. 63, no. 13, pp. 1911–1920, 2003.

[7] N. Angelidis and P. Irving, "Detection of impact damage in CFRP laminates by means of electrical potential techniques," *Composites Science and Technology*, vol. 67, no. 3-4, pp. 594–604, 2007.

[8] A. Baltopoulos, N. Polydorides, L. Pambaguian, A. Vavouliotis, and V. Kostopoulos, "Damage identification in carbon fiber reinforced polymer plates using electrical resistance tomography mapping," *Journal of Composite Materials*, vol. 47, no. 26, pp. 3285–3301, 2013.

[9] J. Cagáň, J. Pelant, M. Kyncl, M. Kadlec, and L. Michalcová, "Damage detection in carbon fiber–reinforced polymer composite via electrical resistance tomography with Gaussian anisotropic regularization," *Structural Health Monitoring*, vol. 18, no. 5-6, pp. 1698–1710, 2019.

[10] T. C. Hou, K. J. Loh, and J. P. Lynch, "Spatial conductivity mapping of carbon nanotube composite thin films by electrical impedance tomography for sensing applications," *Nanotechnology*, vol. 18, no. 31, pp. 315501–315509, 2007.

[11] K. J. Loh, T. C. Hou, J. P. Lynch, and N. A. Kotov, "Carbon nanotube sensing skins for spatial strain and impact damage identification," *Journal of Nondestructive Evaluation*, vol. 28, no. 1, pp. 9–25, 2009.

[12] T. N. Tallman, S. Gungor, K. W. Wang, and C. E. Bakis, "Damage detection and conductivity evolution in carbon nanofiber epoxy via electrical impedance tomography," *Smart Materials and Structures*, vol. 23, no. 4, pp. 045034–045039, 2014.

[13] M. Clausi, E. Toto, S. Botti, S. Laurenzi, V. La Saponara, and M. G. Santonicola, "Direct effects of UV irradiation on graphene-based nanocomposite films revealed by electrical resistance tomography," *Composites Science and Technology*, vol. 183, Article ID 107823, 2019.

[14] T. N. Tallman and D. J. Smyl, "Structural health and condition monitoring via electrical impedance tomography in self-sensing materials: a review," *Smart Materials and Structures*, vol. 29, no. 12, Article ID 123001, 2020.

[15] F. Alberini, D. Bezchi, I. Mannino, A. Paglianti, and G. Montante, "Towards real time monitoring of reacting species and pH coupling electrical resistance tomography and machine learning methodologies," *Chemical Engineering Research and Design*, vol. 168, pp. 369–382, 2021.

[16] F. Li, C. Tan, F. Dong, and J. Jia, "V-net deep imaging method for electrical resistance tomography," *IEEE Sensors Journal*, vol. 20, no. 12, pp. 6460–6469, 2020.

[17] Z. Chen, G. Ma, Y. Jiang, B. Wang, and M. Soleimani, "Application of deep neural network to the reconstruction of two-phase material imaging by capacitively coupled electrical resistance tomography," *Electronics*, vol. 10, no. 9, p. 1058, 2021.

[18] L. Chen, A. Gallet, S. S. Huang, D. Liu, and D. Smyl, "Probabilistic cracking prediction via deep learned electrical tomography," *Structural Health Monitoring*, vol. 21, no. 4, pp. 1574–1589, 2021.

[19] T. Rymarczyk, G. Kłosowski, A. Hoła et al., "Comparison of machine learning methods in electrical tomography for detecting moisture in building walls," *Energies*, vol. 14, no. 10, p. 2777, 2021.

[20] M. Khanal and R. Morrison, "Analysis of electrical resistance tomography (ERT) data using least-squares regression modelling in industrial process tomography," *Measurement Science and Technology*, vol. 20, no. 4, Article ID 045503, 2009.

[21] D. Chakraborty, "Artificial neural network based delamination prediction in laminated composites," *Materials & Design*, vol. 26, no. 1, pp. 1–7, 2005.

[22] Z. Zhang, K. Shankar, T. Ray, E. V. Morozov, and M. Tahtali, "Vibration-based inverse algorithms for detection of delamination in composites," *Composite Structures*, vol. 102, pp. 226–236, 2013.

[23] S. Das, A. N. Srivastava, and A. Chattopadhyay, *Classification of damage signatures in composite plates using one-class SVMs*, pp. 1–19, IEEE, Big Sky, MT, USA, 2007.

[24] I. Tabian, H. Fu, and Z. S. Khodaei, "A convolutional neural network for impact detection and characterization of complex composite structures," *Sensors*, vol. 19, no. 22, p. 4933, 2019.

[25] M. R. P. Elenchezhian, V. Vadlamudi, R. Raihan, K. Reifsnider, and E. Reifsnider, "Artificial intelligence in real-time diagnostics and prognostics of composite materials and its uncertainties–a review," *Smart Materials and Structures*, vol. 30, no. 8, Article ID 083001, 2021.

[26] A. Schmidt, *On delamination crack detection in carbon fiber reinforced polymers using electrical impedance tomography and supervised learning (doctoral dissertation)*, PhD Thesis, Ecole Polytechnique, Montreal, Canada, 2018.

[27] A. Todoroki, "The effect of number of electrodes and diagnostic tool for monitoring the delamination of CFRP laminates by changes in electrical resistance," *Composites Science and Technology*, vol. 61, no. 13, pp. 1871–1880, 2001.

[28] A. Todoroki and M. Ueda, "Low-cost delamination monitoring of CFRP beams using electrical resistance changes with neural networks," *Smart Materials and Structures*, vol. 15, no. 4, pp. 75–84, 2006.

[29] M. Ueda, A. Todoroki, Y. Shimamura, and H. Kobayashi, "Monitoring delamination of laminated CFRP using the electric potential change method: application of normalization method and the effect of the shape of a delamination crack," *Advanced Composite Materials*, vol. 13, no. 3-4, pp. 311–324, 2004.

[30] A. Todoroki, Y. Tanaka, and Y. Shimamura, "Multi-prove electric potential change method for delamination monitoring of graphite/epoxy composite plates using normalized response surfaces," *Composites Science and Technology*, vol. 64, no. 5, pp. 749–758, 2004.

[31] J. Steuben, J. Michopoulos, A. Iliopoulos, and C. Turner, "Inverse characterization of composite materials via surrogate modeling," *Composite Structures*, vol. 132, pp. 694–708, 2015.

[32] A. Iwasaki, A. Todoroki, S. Izumi, and S. Sakai, *Diagnostic Method for Delamination Monitoring of Cfrp Plate Using Kriging Interpolation Method*, vol. 353, pp. 1422–1426, Trans Tech Publication, Switzerland, Europe, 2007.

[33] E. J. Joy, A. S. Menon, and N. Biju, "Implementation of kriging surrogate models for delamination detection in composite structures," *Advanced Composites Letters*, vol. 27, no. 6, Article ID 096369351802700, 2018.

[34] S. Ogihara and N. Takeda, "Interaction between transverse cracks and delamination during damage progress in CFRP cross-ply laminates," *Composites Science and Technology*, vol. 54, no. 4, pp. 395–404, 1995.
[35] P. Díaz-Montiel, L. Escalona-Galvis, and S. Venkataraman, "Kriging and dimension reduction techniques for delamination detection in composites using electrical resistance tomography," *Engineering Optimization*, vol. 1, p. 16, 2021.
[36] L. Selvakumaran and G. Lubineau, "Electrical behavior of laminated composites with intralaminar degradation: a comprehensive micro-meso homogenization procedure," *Composite Structures*, vol. 109, pp. 178–188, 2014.
[37] K. Cheng, D. Isaacson, J. Newell, and D. Gisser, "Electrode models for electric current computed tomography," *IEEE Transactions on Biomedical Engineering*, vol. 36, no. 9, pp. 918–924, 1989.
[38] G. H. Golub and U. Von Matt, "Tikhonov regularization for large scale problems," *Cités*, 1997.
[39] P. Kumar and B. Rai, "Delaminations of barely visible impact damage in CFRP laminates," *Composite Structures*, vol. 23, no. 4, pp. 313–318, 1993.
[40] I. Goodfellow, Y. Bengio, and A. Courville, *Deep Learning*, MIT press, Cambridge, Massachusetts, 2018.
[41] C. M. Bishop, *Pattern Recognition and Machine Learning*, Springer, Berlin/Heidelberg, Germany, 2006.
[42] C. Cortes and V. Vapnik, "Support-vector networks," *Machine Learning*, vol. 20, no. 3, pp. 273–297, 1995.
[43] B. Scholkopf and A. J. Smola, *Learning with Kernels: Support Vector Machines, Regularization, Optimization, and beyond*, Adaptive Computation and Machine Learning Series MIT press, Cambridge, Massachusetts, 2018.
[44] T. K. Ho, "Random decision forests," in *Proceedings of the 3rd International Conference on Document Analysis and Recognition*, pp. 278–282, Cambridge, Massachusetts, July 1995.
[45] L. Breiman, "Random forests," *Machine Learning*, vol. 45, no. 1, pp. 5–32, 2001.
[46] E. Fix and J. L. Hodges, "Discriminatory analysis. Nonparametric discrimination: consistency properties," *International Statistical Review/Revue Internationale de Statistique*, vol. 57, no. 3, pp. 238–247, 1989.
[47] E. Alpaydin, *Introduction to Machine Learning*, MIT press, Cambridge, Massachusetts, 2020.
[48] D. Singh and B. Singh, "Investigating the impact of data normalization on classification performance," *Applied Soft Computing*, vol. 97, Article ID 105524, 2020.
[49] L. Yang and A. Shami, "On hyperparameter optimization of machine learning algorithms: theory and practice," *Neurocomputing*, vol. 415, pp. 295–316, 2020.
[50] F. Pedregosa, G. Varoquaux, and A. Gramfort, "Scikit-learn: machine learning in Python," *Journal of Machine Learning Research*, vol. 12, no. 85, pp. 2825–2830, 2011.
[51] Keras, "Hyperopt: a very simple wrapper for convenient hyperparameter optimization," 2021, https://github.com/maxpumperla/hyperas.
[52] J. Bergstra, B. Komer, C. Eliasmith, D. Yamins, and D. D. Cox, "Hyperopt: a Python library for model selection and hyperparameter optimization," *Computational Science & Discovery*, vol. 8, no. 1, Article ID 014008, 2015.
[53] D. Berrar, "Cross-validation," *Encyclopedia of bioinformatics and computational biology*, vol. 1, pp. 542–545, 2019.
[54] N. Japkowicz and M. Shah, *Evaluating Learning Algorithms: A Classification Perspective*, Cambridge University Press, Cambridge, Massachusetts, 2011.
[55] J. Han, J. Pei, and M. Kamber, *Data Mining: Concepts and Techniques*, Elsevier, Amsterdam, Netherlands, 2011.